

Analysis of numerical models for cavitation on 2D hydrofoil

Keun Woo Shin (kws@mek.dtu.dk), Poul Andersen, Wen Zhong Shen

Dept. of Mechanical Engineering, Technical University of Denmark

1 Introduction

A cavitation model is on the way to be implemented in the incompressible Reynolds-averaged Navier-Stokes equation (RANSE) solver EllipSys3D in order to complement model tests and existing numerical methods for research on marine propellers. EllipSys3D is developed by the Department of Mechanical Engineering at the Technical University of Denmark and the Department of Wind Energy at Risø National Laboratory [6, 9]. As a preliminary step, several cavitation models are implemented in the 2D version of EllipSys3D, and a comparative study between them and an analysis on the influence of some parameters are made.

Numerical models for cavitation can be categorized into two groups: single-phase interface tracking model and multi-phase homogeneous equilibrium model. The former approach, generally adopted for potential flow methods, is less robust, requiring preliminary iterative procedures. The second approach is suitable for RANSE solvers and can be applied to three-dimensional and unsteady flows, including turbulence fluctuations and compressibility effects. Mass transfers between the two phases are based on either a vapor transport equation or a barotropic state law. Three cavitation models using a transport equation and one model using a state law are implemented in EllipSys2D.

2 Mathematical formulation

A single set of RANSE for the mixture flow with the mixture density ρ and the dynamic viscosity μ is solved. The momentum equation is

$$\frac{\partial}{\partial t}(\rho u_i) + \frac{\partial}{\partial x_j}(\rho u_i u_j) - \frac{\partial}{\partial x_j} \left[(\mu + \mu_t) \left(\frac{\partial u_i}{\partial x_j} + \frac{\partial u_j}{\partial x_i} \right) \right] + \frac{\partial p}{\partial x_i} = 0 \quad (1)$$

To avoid interpolating ρ on a cell face, we extract ρ from the derivatives, which results in

$$\rho \left(\frac{\partial u_i}{\partial t} + \frac{\partial}{\partial x_j}(u_i u_j) \right) + u_i \frac{D\rho}{Dt} - \frac{\partial}{\partial x_j} \left[(\mu + \mu_t) \left(\frac{\partial u_i}{\partial x_j} + \frac{\partial u_j}{\partial x_i} \right) \right] + \frac{\partial p}{\partial x_i} = 0 \quad (2)$$

The continuity equation is written in the form of inhomogeneous divergence equation as

$$\frac{\partial u_j}{\partial x_j} = -\frac{1}{\rho} \frac{D\rho}{Dt} \quad (3)$$

Three cavitation models using a transport equation are considered: Singhal's [4, 8], Zwart's [12] and Kunz' [10]. They are some of the most popular models, implemented in the commercial solvers FLUENT, ANSYS CFX and the opensource solver OpenFOAM, respectively.

In Singhal's model [4, 8], a generic transport equation is solved for the vapor mass fraction f as

$$\frac{\partial}{\partial t}(\rho f) + \frac{\partial}{\partial x_j}(\rho u_j f) - \frac{\partial}{\partial x_j} \left(\frac{\mu_t}{Pr_v} \frac{\partial f}{\partial x_j} \right) = -\dot{m} \quad (4)$$

where Pr_v is the turbulent Prandtl number for vapor and \dot{m} is the mass transfer rate per unit volume.

\dot{m} is related to the source term, based on the Rayleigh-Plesset equation as

$$\dot{m} = \begin{cases} -C_e \frac{\sqrt{k}}{T} \rho_l \rho_v \sqrt{\frac{2}{3} \frac{p_v - p}{\rho_l}} (1 - f) & \text{for } p < p_v \\ C_c \frac{\sqrt{k}}{T} \rho_l^2 \sqrt{\frac{2}{3} \frac{p - p_v}{\rho_l}} f & \text{for } p > p_v \end{cases} \quad (5)$$

where C_e, C_c are empirical coefficients for evaporation and condensation, respectively, k is the turbulence kinetic energy and T is the surface tension, $T = 0.0717 \text{ N/m}$. In evaporation for $p < p_v$, the mass in the control volume is decreased when transferring from liquid phase to vapor.

In Zwart's model [12], the transport equation for the vapor volume fraction α_v is solved without diffusion term as

$$\frac{\partial}{\partial t}(\rho_v \alpha_v) + \frac{\partial}{\partial x_j}(\rho_v u_j \alpha_v) = -\dot{m} \quad (6)$$

where

$$\dot{m} = \begin{cases} -C_e \frac{3r_{nuc}\rho_v}{R_B} \sqrt{\frac{2}{3}} \frac{p_v - p}{\rho_l} (1 - \alpha_v) & \text{for } p < p_v \\ C_c \frac{3\rho_v}{R_B} \sqrt{\frac{2}{3}} \frac{p - p_v}{\rho_l} \alpha_v & \text{for } p > p_v. \end{cases} \quad (7)$$

and where R_B is the bubble radius in the nucleation site, $R_B = 10^{-6}$ and r_{nuc} is the nucleation site volume fraction, $r_{nuc} = 5 \cdot 10^{-4}$.

In Kunz' model [10], the transport equation for the liquid volume fraction α_l is solved as

$$\frac{\partial}{\partial t}(\rho_l \alpha_l) + \frac{\partial}{\partial x_j}(\rho_l u_j \alpha_l) = \dot{m} \quad (8)$$

where $\dot{m} = \dot{m}^- + \dot{m}^+$ and

$$\dot{m}^- = \frac{C_e \rho_v \alpha_l \min(0, p - p_v)}{0.5 \rho_l U_\infty^2 t_\infty}, \quad \dot{m}^+ = \frac{C_c \rho_v \alpha_l^2 (1 - \alpha_l)}{t_\infty} \quad (9)$$

and where U_∞, t_∞ are the reference velocity and the time scale, respectively, for which the inlet velocity and C/U_∞ are taken in the hydrofoil case with the chord length C .

The similarity of all three models comes from the relations

$$\rho f = \rho_v \alpha_v = \frac{m_v}{V_t}, \quad \rho(1 - f) = \rho_l \alpha_l = \frac{m_l}{V_t}, \quad -\frac{\rho_l \dot{m}_v}{V_t} = \frac{\rho_v \dot{m}_l}{V_t} = \frac{\rho_v \rho_l \dot{m}}{\rho} \quad (10)$$

where $m_v, m_l, \dot{m}_v, \dot{m}_l$ are the vapor/liquid masses and the vapor/liquid mass transfer rates, respectively, in the computational cell and V_t is the total volume of the computational cell.

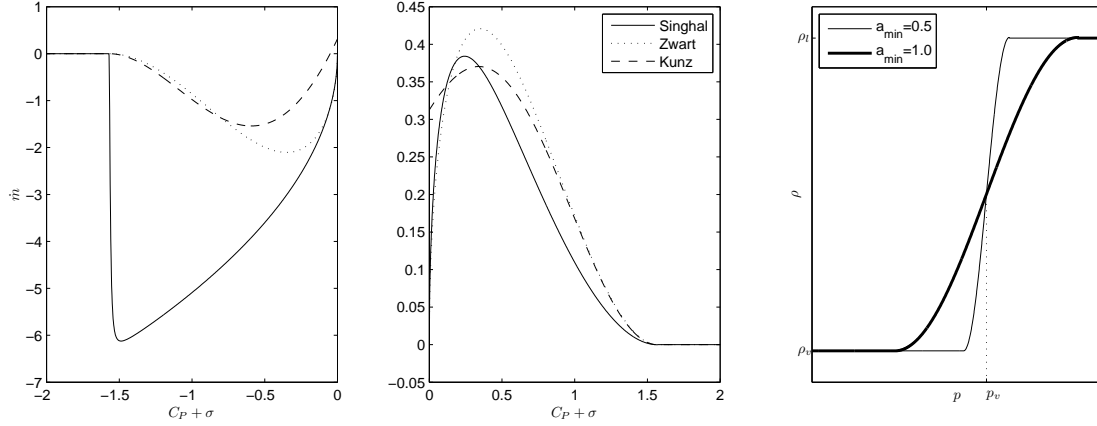


Figure 1: The comparison of \dot{m} from several cavitation models (left,centre) and the barotropic state law (right)

The values of \dot{m} from the three models are given as a function of $C_P + \sigma$ in Figure 1. In computing \dot{m} , the vapor fraction is coupled with p through a barotropic state law in Eq.(15) for a rough comparison. The following values are applied to the coefficients for the comparison in Figure 1 and the computation of the flow around a hydrofoil

Model	Singhal		Zwart		Kunz		
$C_e,$	C_c	0.08,	0.02	0.5,	$5 \cdot 10^{-5}$	2000,	100

The value of \dot{m} from Singhal's model is comparatively large in evaporation, because the value of k is assumed to be 0.1, which is as large as that in highly turbulent regions at the leading edge and right behind the cavity. While the saturation pressure is a bit lower than p_v in Kunz' model, it is exactly p_v in the other ones. The pressure coefficient C_P and the cavitation number σ are

$$C_P = \frac{p - p_\infty}{0.5 \rho_l U_\infty^2}, \quad \sigma = \frac{p_\infty - p_v}{0.5 \rho_l U_\infty^2} \quad (11)$$

The mixture density and the dynamic viscosity are computed as

$$\rho = \alpha_v \rho_v + (1 - \alpha_v) \rho_l, \quad \mu = \alpha_v \mu_v + (1 - \alpha_v) \mu_l \quad (12)$$

By Eq.(12), the momentum and continuity equations are related to the source term of vapor transport equations as

$$\rho \left(\frac{\partial u_i}{\partial t} + \frac{\partial}{\partial x_j} (u_i u_j) \right) + u_i \left(\frac{1}{\rho_l} - \frac{1}{\rho_v} \right) \rho \dot{m} - \frac{\partial}{\partial x_j} \left[(\mu + \mu_t) \left(\frac{\partial u_i}{\partial x_j} + \frac{\partial u_j}{\partial x_i} \right) \right] + \frac{\partial p}{\partial x_i} = 0 \quad (13)$$

$$\frac{\partial u_j}{\partial x_j} = \left(\frac{1}{\rho_l} - \frac{1}{\rho_v} \right) \dot{m} \quad (14)$$

A cavitation model using a barotropic state law [2] is also considered. The mixture density is directly coupled with the pressure through a state law

$$\rho(p) = \begin{cases} \rho_l & \text{for } p > p_v + \Delta p \\ \rho_v & \text{for } p < p_v - \Delta p \\ \rho_v + \Delta \rho \left[1 + \sin \left(\frac{p - p_v}{\Delta \rho a_{min}^2} \right) \right] & \text{elsewhere} \end{cases} \quad (15)$$

where a_{min} is the minimum speed of sound in the liquid/vapor mixture and $\Delta \rho = \frac{\rho_l - \rho_v}{2}$, $\Delta p = \frac{\pi a_{min}^2 \Delta \rho}{2}$. The smaller a_{min} is, the steeper the transition is, as shown in Fig 1 (right).

For all computations, the standard $k - \omega$ turbulence model [11] is used.

3 Implementation

The discretisation is based on the collocated finite volume method. The time derivative is approximated by the second-order backward differentiation scheme.

Since ρ is outside the convective term in Eq.(13) and the divergence term does not contain ρ in Eq.(14), the volume flux on the cell face is calculated using Rhie-Chow interpolation, instead of calculating mass flux. The convective coefficients are estimated by upwind differencing scheme using volume flux and afterwards they are multiplied by ρ on the centre cell. $\left(\frac{1}{\rho_l} - \frac{1}{\rho_v} \right) \rho \dot{m} \Delta V$ is added to the centre-cell coefficient, where ΔV is the volume of computational cell.

The pressure-correction method is based on the SIMPLE scheme, but the sum of volume flux is the source term and the term with \dot{m} is to be considered. Since \dot{m} is dependent on the corrected pressure p' as well, the total mass transfer rate \dot{m}^* taking account of p' is approximated as [5]

$$\dot{m}^* = \frac{\partial \dot{m}}{\partial p} (p + p' - p_v) = p' \frac{\partial \dot{m}}{\partial p} + \dot{m} \quad (16)$$

where p is the pressure obtained from the momentum equation and \dot{m} is found from the source term in the vapor transport equation.

The first term with p' is implicitly treated and the second term \dot{m} is explicitly treated. It results in the integral form of the pressure-correction equation as

$$(A_P + \left(\frac{1}{\rho_l} - \frac{1}{\rho_v} \right) \Delta V \frac{\partial \dot{m}}{\partial p}) p'_P + \sum_{nb} A_{nb} p'_{nb} = \sum_f (\mathbf{u}S)_f - \left(\frac{1}{\rho_l} - \frac{1}{\rho_v} \right) \Delta V \dot{m} \quad (17)$$

The derivative of \dot{m} is

$$\frac{\partial \dot{m}}{\partial p} = \begin{cases} \frac{\dot{m}}{2(p - p_v)} & \text{in Singhal's and Zwart's models} \\ \frac{C_e \rho_v \alpha_l}{0.5 \rho_l U_\infty^2 t_\infty} & \text{for } p < p_v \text{ in Kunz' model} \end{cases} \quad (18)$$

In the model with a state law, we use the derivative term of ρ in Eq.(3) and it is approximated as

$$\frac{1}{\rho} \frac{D\rho}{Dt} = \underbrace{\left[(\rho - \rho^{t-\Delta t}) \frac{\partial}{\partial p} \left(\frac{1}{\rho} \right) + \frac{1}{\rho} \left(\frac{\partial \rho}{\partial p} - \frac{\partial \rho^{t-\Delta t}}{\partial p} \right) \right]}_{\gamma} (p + p' - p_v) \quad (19)$$

where $\rho^{t-\Delta t}$, $\frac{\partial \rho}{\partial p}^{t-\Delta t}$ is the density and the derivative of density, respectively, at the previous time-step and the derivatives are

$$\frac{\partial \rho}{\partial p} = -\frac{1}{a_{min}^2} \cos \left(\frac{p - p_v}{\Delta \rho a_{min}^2} \right), \quad \frac{\partial}{\partial p} \left(\frac{1}{\rho} \right) = -\frac{1}{\rho^2} \frac{\partial \rho}{\partial p} \quad (20)$$

Accordingly the pressure-correction equation becomes

$$(A_P + \gamma \Delta V) p'_P + \sum_{nb} A_{nb} p'_{nb} = \sum_f (\mathbf{u}S)_f - \gamma \Delta V (p - p_v) \quad (21)$$

4 Numerical results

The cavitating flow around the NACA66(mod) hydrofoil section is numerically solved, applying the different cavitation models. The section geometry and Reynolds number correspond to the ones experimentally investigated in [7]. The O-type mesh consists of 32768 cells in the computational domain with the extent of $20C$. The first-cell height on the wall corresponds to $y^+ \simeq 2$, as shown in Figure 2. The angle of inlet flow is adjusted to the angle of attack α .

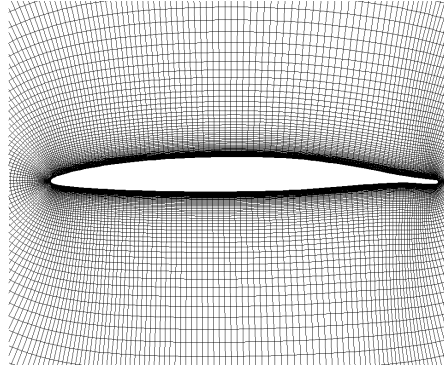


Figure 2: Computational grid

$\rho_l/\rho_v = 10000$, $\mu_l/\mu_v = 100$ are used. As shown in Figure 3 (right), the results are consistent for $\rho_l/\rho_v > 1000$. The time-step size is set to $1 \cdot 10^{-5}C/U_\infty$, corresponding to the local Courant number of $0.005 \sim 0.2$.

Numerical results for two cases of $\alpha = 4^\circ$, $\sigma = 0.91$, $\alpha = 1^\circ$, $\sigma = 0.38$ are obtained. In Singhal's model, $Pr_v = 2.0$ is used in order to increase vapor convection rather than diffusion, unlike $Pr_v = 0.7 \sim 1.0$ in [4]. In the present implementation, the Singhal's model does not work without diffusion term. In Kunz' model, the solution is converged for $\rho_l/\rho_v \leq 1000$, but it is unstable for high C_e . It seems to be because a constant value is applied for $\frac{\partial m}{\partial p}$ in the pressure-correction equation. In a state law, a_{min} is gradually decreased from 0.5 to 0.2 and it does not work $a_{min} < 0.2$.

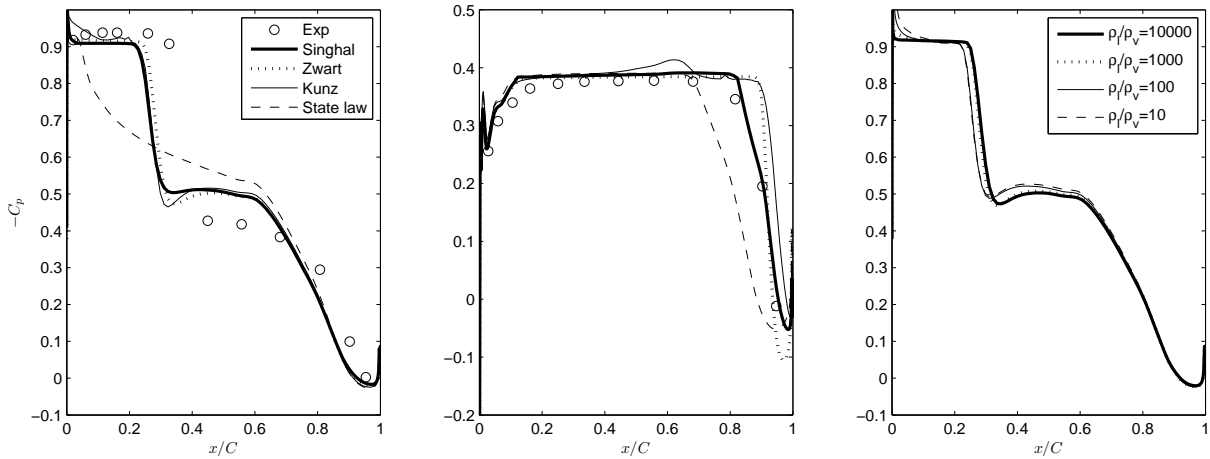


Figure 3: $-C_P$ on the suction side of a hydrofoil from different cavitation models for $\alpha = 4^\circ$, $\sigma = 0.91$ (left), $\alpha = 1^\circ$, $\sigma = 0.38$ (centre) and $-C_P$ from Zwart's model with varying ρ_l/ρ_v for $\alpha = 4^\circ$, $\sigma = 0.91$ (right)

The cavity size oscillates periodically for all the models except in that with a state law. $-C_P$ and α_v at the maximum cavity size are shown in Figure 3 and 4, respectively. The numerical results are summarized as

1. $-C_P$ from the models with a vapor transport equation generally agrees well with that from the experiment in both cases. The distribution of $-C_P$ differs from that from the experiment at the cavity end for $\alpha = 1^\circ$. It can be adjusted by handling the value of C_e .

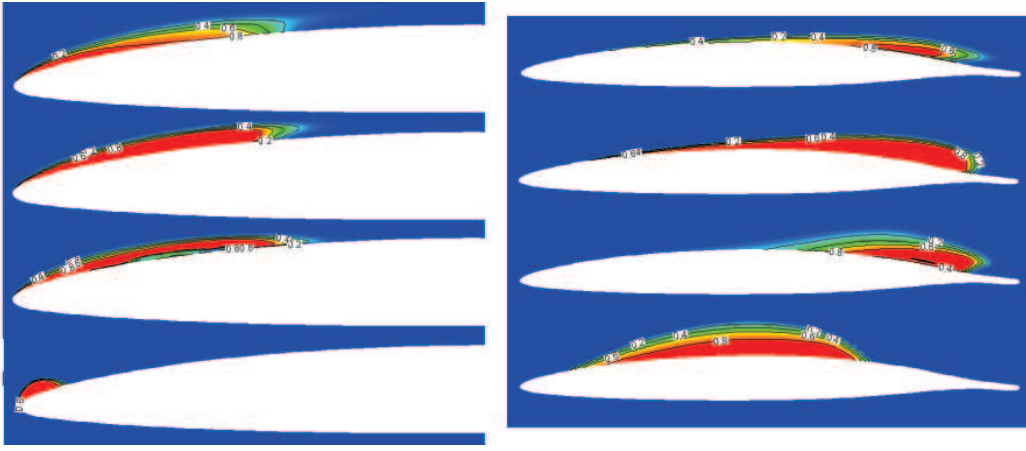


Figure 4: α_v from Singhal's, Zwart's, Kunz' models and the state law (from top to bottom) for $\alpha = 4^\circ$, $\sigma = 0.91$ (left) and $\alpha = 1^\circ$, $\sigma = 0.38$ (right)

2. The cavity size is a bit shorter than that from the experiment for $\alpha = 4^\circ$. The experiment may have a larger effective α due to the limited tunnel length and a different turbulence characteristics.
3. $-C_P$ behind the cavity is larger than that from the experiment for $\alpha = 4^\circ$. It seems to be because the cloudy cavitation is not realized. Different turbulence models should be tried.
4. For the model with a state law, the cavity is not convected and hence the cavity remains at the low-pressure region from the solution without the cavitation model.
5. The distribution of α_v differs, as the distribution of \dot{m} as a function of p differs.

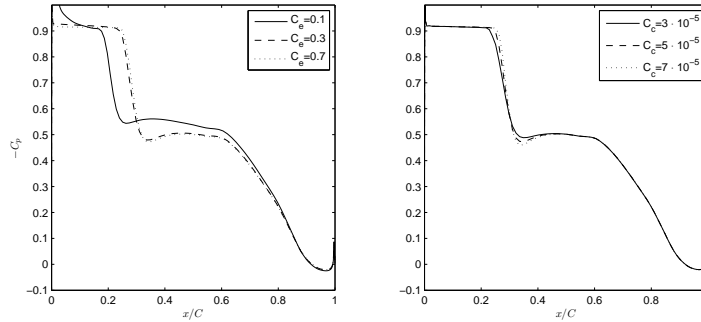


Figure 5: $-C_P$ from Zwart's model with $C_c = 5 \cdot 10^{-5}$ (left) and with $C_e = 0.5$ (right)

With Singhal's and Zwart's models, shown to be rather stable and accurate, we analyze the influence of C_e, C_c for the case with $\alpha = 4^\circ, \sigma = 0.91$. The results are shown in Figure 5 and 6. There are certain upper and lower limits on C_e, C_c for the numerical solution to be stable. It is summarized as

1. When C_e is smaller than a certain value, it takes more time for the cavity to be formed behind the low pressure region at the leading edge and the cavity size is rather small.
2. When C_e is larger than a certain value, the solution is converged and no change occurs.
3. The smaller C_c is, the cavity is condensed more gradually with lower pressure gradient at the cavity end.

5 Conclusion

Several cavitation models are implemented in EllipSys2D and the numerical results show that Singhal's and Zwart's models are stable and accurate in our implementation. But the cloudy cavitation is not well realized. The cavitation model is to be tested with different types of turbulence models.

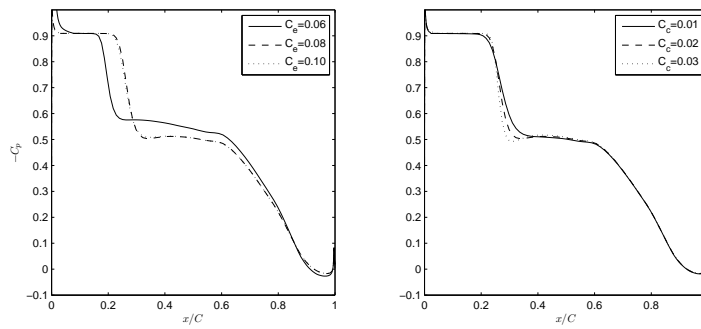


Figure 6: $-C_P$ from Singhal's model with $C_c = 0.02$ (left) and with $C_e = 0.08$ (right)

A way to improve the \dot{m} derivative term in the pressure-correction equation for Kunz' model needs to be devised for achieving higher stability. The remedy for including vapor convection in the model with a barotropic state law needs to be found out.

The coefficients C_e, C_c in evaporating and condensing rates, respectively, are shown to work according to physics and the cavitation strength can be adjusted by calibrating them.

Acknowledgement

The advices from the Institute of Fluid Dynamics and Ship Theory in Technical University of Hamburg-Harburg are gratefully acknowledged.

References

- [1] Frikha, S., Coutier-Delgosha, O., Astolfi, J. A. "Influence of the cavitation model on the simulation of cloud cavitation on 2D foil section," Int. J. of Rotating Machinery, 2008
- [2] Hoeijmakers, H. W. M., Janssens, M. E., Kwan, W., "Numerical simulation of sheet cavitation," 3rd Int. Symp. on Cav., 1998
- [3] Kim, S. E., Brewton, S., "A multiphase approach to turbulent cavitating flows," 27th Symp. on Naval Hydrodyn., 2008
- [4] Rhee, S. H., Kawamura, T., Li, H. Y., "Propeller cavitation study using an unstructured grid based Navier-Stokes Solver," ASME J. Fluids Eng., 2005
- [5] Maquil, T., "Simulation von instationären kavitierenden Strömungen mit Hilfe von Mischungsbruchansätzen," Kleine Studienarbeit, TUHH, 2007
- [6] Michelsen, J. A., *Basis3D- A platform for development of multiblock PDE solvers*, Technical Report AFM 92-05, DTU, Denmark, 1992
- [7] Shen, Y. J. and Dimotakis, J. S., "The influence of surface cavitation on hydrodynamics forces," 22nd ATTC, 1989
- [8] Singhal, A. K., Athavale, M. M., Li, H. Y., Jiang, Y., "Mathematical basis and validation of the full cavitation model," ASME J. Fluids Eng., 2002
- [9] Sørensen N. N., *General purpose flow solver applied to flow over hills*, Risø, 2003
- [10] Wikstrom, N., "Modeling of cavitating flow around a stationary/moving wing profile," 43rd AIAA Aerospace Sc. Meeting, Reno, NV, 2005
- [11] Wilcox, D. C. *Turbulence modeling for CFD*, DCW Industries, Inc., La Canada, CA, 2nd ed., 1994
- [12] Zwart, P. J., Gerber, A. G., Belamri T., "A two-phase flow model for predicting cavitation dynamics," ICMF, 2004